bioRxiv preprint doi: https://doi.org/10.1101/2023.03.06.531250; this version posted March 6, 2023. The copyright holder for this preprint (which was not certified by peer review) is the author/funder, who has granted bioRxiv a license to display the preprint in perpetuity. It is made available under aCC-BY 4.0 International license.

Efficient clathrin-mediated entry of enteric adenoviruses in human duodenal cells

Miriam Becker[1,2,3,4]*, *Noemi Dorma*[2,3], *Dario Valter Conca*[2,3], *Nitesh Mistry*[2,3], *Marta Bally*[2,3], *Niklas Arnberg*[2,4]¶, *and Gisa Gerold*[1,2,3]¶*

[1]Department of Biochemistry & Research Center for Emerging Infections and Zoonoses (RIZ), University of Veterinary Medicine Hannover, Hannover, Germany

[2]Department of Clinical Microbiology, Umeå University, Sweden

[3]Wallenberg Centre for Molecular Medicine (WCMM), Umeå University, Sweden

[4]Molecular Infection Medicine Sweden (MIMS), Umeå University, Sweden

* Corresponding authors

E-mail: miriam.becker@tiho-hannover.de (MiB); gisa.gerold@tiho-hannover.de (GG)

¶*shared last authorship*

Keywords: enteric adenovirus, virus entry, single particle tracking, clathrin-mediated endocytosis, electron microscopy

bioRxiv preprint doi: https://doi.org/10.1101/2023.03.06.531250; this version posted March 6, 2023. The copyright holder for this preprint (which was not certified by peer review) is the author/funder, who has granted bioRxiv a license to display the preprint in perpetuity. It is made available under aCC-BY 4.0 International license.

Abstract

Enteric adenovirus types F40 and 41 (EAdVs) are a leading cause of diarrhea and diarrhea-associated death in young children and have recently been proposed to cause acute hepatitis in children. Unlike other adenoviruses, EAdVs exhibit hitherto a strict tropism for gastrointestinal tissues with, to date, unknown infection mechanism and target cells. In this study, we turn to potentially limiting host factors by comparison of EAdV entry in cell lines with respiratory and intestinal origin by cellular perturbation, virus particle tracking and transmission electron microscopy. Our analyses highlight kinetic advantages in duodenal HuTu80 cell infection and reveal a larger fraction of mobile particles, faster virus uptake and infectious particle entry in intestinal cells. Moreover, EAdVs display a dependence on clathrin- and dynamin-dependent pathways in intestinal cells. Detailed knowledge of virus entry routes and host factor requirements is essential to understand pathogenesis and develop new countermeasures. Hence, this study provides novel insights into the entry mechanisms of a medically important virus with emerging tropism in a physiologically relevant cell line.

Author Summary

Enteric adenoviruses have historically been difficult to grow in cell culture, which resulted in lack of knowledge of host factors and pathways required for infection of these medically relevant viruses. Previous studies in non-intestinal cell lines showed slow infection kinetics and generated comparatively low virus yields compared to other adenovirus types. We suggest duodenum derived HuTu80 cells as a superior cell line for studies to complement efforts using complex intestinal tissue models. We show that viral host cell factors required for virus entry differ between cell lines from distinct origins and demonstrate the importance of clathrin-mediated endocytosis.

bioRxiv preprint doi: https://doi.org/10.1101/2023.03.06.531250; this version posted March 6, 2023. The copyright holder for this preprint (which was not certified by peer review) is the author/funder, who has granted bioRxiv a license to display the preprint in perpetuity. It is made available under aCC-BY 4.0 International license.

Introduction:

Human enteric adenovirus type 40 and 41 (EAdV) are the only human members of species F of the growing *Adenoviridae* family, which currently has over 110 members divided in species A-G (1,2). While other adenovirus types cause disease in eyes, airways, liver, adenoids and/or urinary tract, EAdVs have a pronounced tropism for the gastrointestinal tract (3) and are one of the leading causes for acute virus gastroenteritis and associated death in children below 5 years of age (4,5). In 2022, more than 1,000 cases of acute hepatitis of unknown cause occurred in children worldwide, including 22 deaths (6). In UK, adenoviruses were detected in 122 of 183 cases (69%) and, with human adenovirus type 41 (AdV41) being the most common (92.3%) adenovirus type detected in blood (7), suggesting a potential novel role for these viruses.

Despite being a common cause of disease in humans, the interplay of host factors and virus entry requirements for EAdVs is largely unknown. The main reason for this is that EAdV have been difficult to isolate and amplify to high viral titer in cell culture (8,9). The icosahedral capsid of adenoviruses consists of three capsid proteins, where the major capsid protein, hexon, is the main structural component. Pentamers of viral penton proteins are located at the tips of the icosahedral vertices and from their centers, trimeric fiber proteins are protruding (10). In contrast to other AdVs, EAdVs carry two distinct fiber proteins of different length (11,12), which mediate interaction with surface attachment factors and binding receptors, heparan sulfate proteoglycans (HSPG) and coxsackie- and adenovirus receptor (CAR), respectively (13,14). All other AdV types interact with cell-surface integrins via an RGD-motif in the penton protein, which aids in endocytic uptake and uncoating of the virus (15,16). EAdVs, however, lack such conserved RGD-motifs and therefore interact with laminin-binding integrins instead (17). The overall EAdV structure is largely resistant to pH changes that resemble passage through the stomach, which may contribute to the gastrointestinal tropism (18,19). Due to their fastidious nature, most studies have been conducted in A549 and HEK293 cells where EAdV entry was slow, occurred in a clathrin-independent manner, and with inefficient

bioRxiv preprint doi: https://doi.org/10.1101/2023.03.06.531250; this version posted March 6, 2023. The copyright holder for this preprint (which was not certified by peer review) is the author/funder, who has granted bioRxiv a license to display the preprint in perpetuity. It is made available under aCC-BY 4.0 International license.

endosomal escape (20,21). Previous attempts to study EAdV infection in human ileal organoids succeeded in virus amplification but failed to identify EAdV target cells (22). This highlights the need to identify the molecular determinants responsible for the specific EAdV tissue tropism by exploring novel infection models.

In this study, we compared the EAdV infection kinetics and cell entry pathway in duodenal HuTu80 cell lines to lung-derived A549 cell lines to identify possible cell type specific advantages in cells derived from the gastrointestinal tract. We found that infectious internalization was faster and clathrin-dependent in HuTu80 cells highlighting the need for tissue specific virus infection studies. Our results suggest that the clinically relevant but understudied species F adenovirus carry traits not seen in other adenoviruses, which enable efficient entry in cells of the gastrointestinal tract.

Results

Faster uptake and infection kinetics of EAdVs in duodenal HuTu80 cells

With the aim to explore the host cell requirements of enteric adenoviruses (EAdVs) in duodenal HuTu80 and lung-derived A549 cells, we confirmed susceptibility of both cell lines to AdV40, AdV41, and AdV5 (S1 Fig.A-C). To study AdV entry in more detail, we established an uptake assay based on dual-labeling of virus particles (Fig. 1A). In brief, AF488 fluorescently labeled AdVs were bound to cells at 4°C followed by a shift to 37°C to allow internalization. To distinguish intracellular and extracellular virus particles, cells were shifted back to 4°C to inhibit further internalization, and extracellular particles were visualized with an anti-AF488 primary antibody and AF568 secondary antibody without fixation. Thereafter live cells were analyzed by flow cytometry (Fig. 1C-E) for total virus signal (AF488) and extracellular fraction (AF568)

bioRxiv preprint doi: https://doi.org/10.1101/2023.03.06.531250; this version posted March 6, 2023. The copyright holder for this preprint (which was not certified by peer review) is the author/funder, who has granted bioRxiv a license to display the preprint in perpetuity. It is made available under aCC-BY 4.0 International license.

or fixed and stained for microscopy analysis (Fig. 1G and Fig. 1H). To validate the assay specificity, fluorescently labeled AdV40 was bound to and incubated with cells at 4°C or allowed to directly internalize for 4 h at 37°C before staining with subsequent fixation (Fig. 1B). Analysis by confocal microscopy revealed that extracellular particles were double stained (Fig. 1B top row), whereas internalized particles were protected from anti-AF488 staining (Fig. 1B bottom row). EAdV were described to internalize slowly in A549 and HEK293 cells as compared to other AdV types (20,21). We confirmed by flow cytometry that uptake of EAdV into A549 cells was slow and reached 90-100% after 2-3 h, whereas 75% of AdV5 particles were already taken up after 30 min (Fig. 1C-E). We observed that both AdV40 and AdV41 entered HuTu80 about twice as fast than into A549 cells. In contrast, AdV5 entered into HuTu80 and A549 cells equally fast (Fig. 1E). This suggested a cell line specific advantage for EAdVs in HuTu80 cells with regard to virion internalization.

Figure 1: Uptake and infection kinetics of EAdV is faster in duodenal HuTu-80 cells. A) Scheme of the dual label uptake assay to distinguish internalized from extracellular AdVs. AF488-AdVs were bound to target cells in suspension followed by internalization. Extracellular virus accessible to anti-AF488 antibody staining showed a dual labeling measurable by flow cytometry. B) Validation of uptake of AF488-labeled AdV40 bound to A549. Dual staining depended on extracellular localization as in the top panel with the binding only control. Scale bar: 10 µm. C-E) Uptake assay of AdV40 (C), AdV41 (D), and AdV5 (E) in A549 (black) and HuTu80 (red) cells assessed through shifts in mean fluorescence intensities by flow cytometry. F) Scheme of an infectious internalization assay to determine kinetics of infectious uptake of AdVs. G/H) AdVs were bound to and internalized into A549 or HuTu80 cells. Extracellular EAdV particles washed at low pH, whereby only internalized particles led to infection. Error bars show standard error of the mean. Statistical significance by unpaired students t-test: *: $p<0.05$.

bioRxiv preprint doi: https://doi.org/10.1101/2023.03.06.531250; this version posted March 6, 2023. The copyright holder for this preprint (which was not certified by peer review) is the author/funder, who has granted bioRxiv a license to display the preprint in perpetuity. It is made available under aCC-BY 4.0 International license.

To investigate the relevance of this advantage for productive virus uptake, we next developed an infectious uptake assay, where EAdVs were bound at 4°C, then allowed to enter cells at 37°C for different durations. After the respective internalization time, we rendered extracellular particles non-infectious by low pH wash (S2 Fig.) and quantified successful viral hexon production as a correlate of productive entry 48 h post infection. Both AdV40 and AdV41 reached higher infection levels in HuTu80 cells as compared to A549 cells, especially after washes at early time points between 2 h and 6 h of internalization (Fig. 1G/H). Thus, infectious EAdV internalization was faster in HuTu80 cells as compared to A549 cells. These results suggest that duodenal cells are a more suitable cell model to study EAdV entry than previously used cell lines.

EAdVs display heterogeneous motion and increased free diffusion with time and in HuTu80

After establishing that EAdV entry is significantly faster in HuTu80 cells than in A549, we investigated if virus particle motion after attachment to the cell surface also differed between cell lines. To this end we tracked single particles of fluorescently labeled AdV by highly inclined and laminated optical sheet (HILO) microscopy (23). We incubated A549 and HuTu80 cells with AF488-AdV5/40/41 for 5 min at 37°C and observed virus motion on cells at 5 min and 30 min after removal of virus inoculum. We acquired videos at 10 frames/s for two min each. The tracks were analyzed using a divide-and-conquer moment scaling spectrum (DC-MSS) algorithm (24,25), which allowed us to subdivide each track into segments displaying distinct motion patterns. Four motion types were considered in the analysis: immobile particles, confined diffusion, free diffusion, and directed motion. Representative examples of the acquired tracks are shown in Fig. 2A. We first analyzed the diffusion coefficient for each motion type. Surprisingly, no clear differences between AdV types or cell lines were observed (S3 Fig.). Both free and confined diffusion had a mean diffusion coefficient between

bioRxiv preprint doi: https://doi.org/10.1101/2023.03.06.531250; this version posted March 6, 2023. The copyright holder for this preprint (which was not certified by peer review) is the author/funder, who has granted bioRxiv a license to display the preprint in perpetuity. It is made available under aCC-BY 4.0 International license.

0.008 and 0.02 $\mu m^2/s$, while directed motion exhibits slightly higher values between 0.015 and 0.035 $\mu m^2/s$. These values were comparable to values reported previously for AdV2 internalization (16). In all cases and for all motion types, we observed large variations in the diffusion coefficient values, with standard deviations >0.02 μm/s and single recorded values ranging between $5x10^{-5}$ to 0.05 $\mu m^2/s$. This heterogeneity in the diffusion coefficient value can be attributed to the different possible interactions between cell components and the virus, which result in various levels of mobility.

Figure 2: EAdVs display increased free diffusion with time and on HuTu80 cells. A) Representative tracks produced by AdV particles moving on live cells. The colors show the results of the track segmentation algorithm. The number next to each track is its average motion coefficient ranging between 0, for a fully immobile track, and 3, for directed motion. B-C) Fraction of the total track time spent by AdV particles in confined (B) and free (C) diffusion, after 5 and 30 min from the removal of the inoculum and on A549 and HuTu80. Grey dots indicate the value for each recorded video. Error bars indicate the standard error of the mean. Statistical significance determined using two-way ANOVA test: *: $p<0.05$, **: $p<0.01$, ***: $p<0.001$, ****: $p<0.0001$. D-F) Truncated violin plot showing the distribution of full tracks according to their average motion coefficient on A549 and HuTu80 cells after 5 and 30 min from the removal of the inoculum for AdV40 (D), AdV41 (E) and AdV5 (F). Single tracks are shown as grey dots. G) Percentage of the tracks in (D-F) with an average motion coefficient higher than 1.5, i.e. displaying a motion dominated by free and directed diffusion.

We then focused on the relevance of each motion type, measured as the fraction of time spent by the particles in each of those. We observed in all cases a prevalence of confined motion (from 40% to 68% of the total time) followed by free diffusion and immobile particles, while directed motion only relegated to a few percent of the total time tracked (S4 Fig. A). Noteworthy, the analysis of the fraction of total time likely underestimates the importance of

bioRxiv preprint doi: https://doi.org/10.1101/2023.03.06.531250; this version posted March 6, 2023. The copyright holder for this preprint (which was not certified by peer review) is the author/funder, who has granted bioRxiv a license to display the preprint in perpetuity. It is made available under aCC-BY 4.0 International license.

fast but short-lived motion segments. In these segments, AdV particles might cover large distances making them significant in the overall dynamic of the interaction with the host cell. To further explore this possibility, we considered the distance travelled by the particle in each segment as the distance between the two furthest points in each track segment (as visualized in S4 Fig. D/E). In this case, free diffusion becomes the most prevalent motion type, and the importance of directed motion becomes evident, accounting for as much as 20% of the distance travelled by AdV5 particles on A549 cells (S4 Fig. F). We then compared the variations in the frequency of each motion type between cell lines and time points for all three viruses. The behavior of AdV5 shows little dependence on time and cell type, with a small increase of free motion in HuTu80 cells as compared to A549 and a respective reduction of immobile particles (Fig. 2B and S4 Fig. B). This time-independence supports the internalization data in Fig. 1 indicating a fast kinetics for AdV5 internalization regardless of the cell type. Particularly noteworthy is the behavior of AdV40 and AdV41. As shown in Fig. 2B-C, when comparing motion on A549 and HuTu80, we observe a significant increase in free diffusion (from a fraction of 0.25 to 0.42 and from 0.19 to 0.38 after 30 minutes for AdV40 and AdV41, respectively) and reduction in confined motion (from 0.60 to 0.45 and from 0.59 to 0.52 for AdV40 and AdV41). For AdV41, we also observe a clear reduction of immobile particles, which is not present for AdV40 (S4 Fig. B). This indicates a much more dynamic behavior of EAdV particles on intestinal cells. In addition, we observed a significant increase in mobility with time for both AdV40 and AdV41 on HuTu80 cells. The free motion fraction increased by around 10% of the total time for both EAdVs, reaching similar levels measured for AdV5 (Fig. 2B), while the confined fraction was reduced simultaneously (Fig. 2C). We did not observe a significant variation for directed motion (S2 Fig. C), most probably due to the reduce sample size. In sum, we show that EAdVs show an overall increased movement dynamics during the attachment and entry process in intestinal cells.

Combining all segments of a motion type from all tracks, however, does not consider the possible heterogeneity in the diffusion behavior and mobility between single particles. To investigate this, we developed a parameter that describes the overall dominant motion type for

bioRxiv preprint doi: https://doi.org/10.1101/2023.03.06.531250; this version posted March 6, 2023. The copyright holder for this preprint (which was not certified by peer review) is the author/funder, who has granted bioRxiv a license to display the preprint in perpetuity. It is made available under aCC-BY 4.0 International license.

each track. We scored every motion type with an integer number between 0 and 3 in increasing order of mobility and defined the “average motion coefficient” (AMC) as the time average of the motion types displayed by each track. In this way, tracks receive a fractional number between 0 and 3, with values close to 1 indicating a predominantly immobile/confined motion and around 2 for free diffusion and directed motion. Examples of AMC scores are shown in Fig. 2A, while the distribution of the AMC for all tracks is shown in Fig. 2D for AdV40 and Fig. 2E for AdV41. In all conditions, a population is present around a value of 1, comprising the particles that display almost exclusively confined motion. This is the only major peak present for A549 cells, with only a small tail reaching AMC values close to 2. Particles on HuTu80 cells instead are characterized by a more heterogeneous track distribution, which is again dependent on the observation time. After 5 min incubation, only one major peak is present around 1, however, the distribution appears significantly broader towards higher scores than in the A549 case. At 30 min a second population appears centered around 2 for both EAdVs. This indicates that rather than a homogeneous increase of the free diffusion mode shared by most particles, the larger free-diffusing fraction is due to the appearance of a population of mostly freely diffusing particles, while others remain immobile or restricted in their motion. For AdV5, we observe a broad distribution extending in into large AMC values in all conditions and the presence of the second peak around an AMC value of 2 in all cases except for A549 cells after 5 min (Fig. 2F). Finally, we estimated the size of the two populations by a simple thresholding at an AMC score of 1.5. After 30 min the number of tracks undergoing mostly free diffusion is 2.8 times higher for HuTu80 than for A549 in the case of AdV40 and 3.4 times higher for AdV41. No clear increase is observed for AdV5 when comparing the two cell lines (Fig. 2G). At the early time point (5 min), the difference between the two cell lines is even larger (6-fold) for EAdV41, while AdV40 shows little difference between the two cell lines and AdV5 a 2-fold increase. Taken together, this indicates that the faster internalization observed for EAdV on HuTu80 cells correlates with an increase in overall mobility. This in turn is driven by the emergence of a highly mobile population, which increases with time.

bioRxiv preprint doi: https://doi.org/10.1101/2023.03.06.531250; this version posted March 6, 2023. The copyright holder for this preprint (which was not certified by peer review) is the author/funder, who has granted bioRxiv a license to display the preprint in perpetuity. It is made available under aCC-BY 4.0 International license.

Kinetic advantage is reflected in intracellular localization of EAdVs

The observation that EAdVs entered HuTu80 cells rapidly, prompted us to investigate EAdV localization in HuTu80 (Fig. 3B) versus A549 (Fig. 3A) after 12.5 min, 2 h and 6 h of internalization by transmission electron microscopy. We consistently observed virus particles binding to flat membrane regions or at the tip of cellular protrusions (Fig. 3A/B “binding” and Fig. 3C blue) at all time-points and for both cell lines. Moreover, virus particles associated with curved membranes with and without clathrin coat were observed in all experimental conditions (Fig. 3A/B “endocytic pit” and Fig. 3C green); virus particles were also found in intracellular vesicles or endosomes (Fig. 3A/B “endosome” and Fig. 3C red). In rare cases virus particles appeared without endosomal membrane coat in the cytosol indicating successful endosomal escape, however these events were not observed in A549 cells at 12.5 min of internalization (Fig. 3A/B “cytosolic” and Fig. 3C yellow). Quantification of these four virus localizations (plasma membrane, endocytic pit, endosome, and cytosol) confirmed that at these early time points a greater fraction of viruses localized to intracellular compartments of HuTu80 as compared to A549 cells. This was most obvious at 2 h internalization, where only 15%-25% of AdV40 and AdV41 were found intracellularly in A549 cells, but 40%-60% in HuTu80 cells (Fig. 3D vs. Fig. 3E at 2 h). These results are well in line with our observations in flow cytometry and infection assays (Fig. 1). In summary, our data suggest that duodenal HuTu80 cells provide a cell type specific advantage for EAdV infectious entry and may serve as an improved cell culture model.

Figure 3: EAdV uptake observed in transmission electron microscopy mirrors kinetic advantage. A) Panel of exemplary cropped TEM images from A549 cells incubated with AdV40 (left) or AdV41 (right) and classification of virus localization into categories: bound (blue), endocytic pit (green), internalized (red), and cytosolic (yellow); B) Panel of exemplary

bioRxiv preprint doi: https://doi.org/10.1101/2023.03.06.531250; this version posted March 6, 2023. The copyright holder for this preprint (which was not certified by peer review) is the author/funder, who has granted bioRxiv a license to display the preprint in perpetuity. It is made available under aCC-BY 4.0 International license.

TEM images as in A) from HuTu80 cells. Scale bars: 100 nm. C) Scheme for scoring of localization of AdV particles on cells in the EM experiments; D/E) Quantification of uptake of EAdVs into A549 (D) and HuTu80 (E) cells. At least n=50 virus particles were classified per time point.

EAdVs enter cells in a clathrin- and actin-dependent manner

Enteric adenovirus entry was previous studied in A549 and HEK293 cells and has been described to be clathrin-independent in HEK293 (20,21). The faster EAdV-specific uptake kinetics in duodenal HuTu80 cells prompted us to study their cell entry pathways using the flow cytometry-based uptake assay (Fig. 1A) in presence of small molecule inhibitors of endocytic pathways. Cells were detached with PBS/EDTA and suspended in growth medium with small molecule inhibitors for 30 min pretreatment. We next added virus particles to cells for 1 h at 4°C in presence of the inhibitors. Thereafter, the virus inoculum was removed and cells were resuspended in medium with inhibitor and shifted to 37°C for internalization for 4 h. We used an anti-AF488 antibody staining on live cells at 4°C as above, to detect remaining extracellular virions.

Clathrin-mediated endocytosis (CME) is a well characterized endocytic pathway (26) and used for cell entry by several AdVs (27). Pitstop2 blocks attachment of clathrin triskelions to the forming endocytic pit (28) and thereby inhibits CME. In our virus entry assay, pitstop2 reduced uptake of EAdVs dose-dependently to a maximum of 50% internalization in HuTu80 cells but interestingly did not affect uptake into A549 cells (Fig. 4A/B). These findings suggested a possible difference between entry pathways in A549 and HuTu80 and prompted us to explore the involvement of CME further. To that end we tested the involvement of dynamins, which are GTPases acting as important scission factors during endocytic vesicle formation in CME, but also during caveolae-dependent endocytosis and phagocytosis (29). We assessed the involvement of dynamins in EAdV endocytosis by inhibition of its GTPase function by dynasore (30). Dynasore inhibited EAdV uptake dose-dependently in both cell

bioRxiv preprint doi: https://doi.org/10.1101/2023.03.06.531250; this version posted March 6, 2023. The copyright holder for this preprint (which was not certified by peer review) is the author/funder, who has granted bioRxiv a license to display the preprint in perpetuity. It is made available under aCC-BY 4.0 International license.

lines. Specifically, dynasore reduced internalization rates to below 50% residual uptake for all viruses at the highest inhibitor concentration (Fig. 4C/D). As dynasore treatment affects several pathways, the larger reduction in internalization observed as compared to pitstop2 indicates that several endocytic pathways are active in parallel during uptake.

Figure 4: EAdV uptake depends on clathrin, dynamins and actin. Relative EAdV uptake in A549 (black) and HuTu80 (red) cells in the presence of clathrin-inhibitor pitstop-2 (A/B), dynamin-inhibitor dynasore (C/D), cholesterol-depleting agent methyl-beta-cyclodextrin (E/F), with actin-perturbating cytochalasin D (G/H) at indicated concentrations, compared to vehicle control (DMSO). Error bars indicate the standard error of the mean. Statistical significance determined using two-way ANOVA test: *: $p<0.05$, **: $p<0.01$, ***: $p<0.001$, ****: $p<0.0001$.

Next, we assessed whether EAdV entry required membrane cholesterol in addition to clathrin and dynamin. Cholesterol is an important membrane organizer and its depletion can affect membrane dynamics and domain formation (31,32). We used methyl-β-cyclodextrin (mβCD) to sequester cholesterol from membranes (33,34), which only mildly affected EAdVs uptake (Fig. 4E/F). This suggests that cholesterol-rich domains or cholesterol-dependent membrane dynamics are not involved in EAdV uptake.

Finally, we probed for a role of actin in EAdV entry. Actin dynamics affect, among other processes, the maintenance of membrane rigidity, cell movement and intracellular transport (35). We utilized cytochalasin D (cytoD) to perturb the dynamics of the actin cytoskeleton by blocking actin filament elongation (36). Perturbation of dynamic actin remodeling by cytoD reduced EAdV uptake dose-dependently to maximally 50% residual particle uptake in both cell lines (Fig. 4G/H). This finding is expected, as actin regulates several cellular processes and thus can affect virus uptake at several stages.

bioRxiv preprint doi: https://doi.org/10.1101/2023.03.06.531250; this version posted March 6, 2023. The copyright holder for this preprint (which was not certified by peer review) is the author/funder, who has granted bioRxiv a license to display the preprint in perpetuity. It is made available under aCC-BY 4.0 International license.

In summary, our data suggest that EAdV entry is clathrin-independent in A549 cells, but clathrin and dynamin dependent in HuTu80, pointing towards CME as the major uptake route in duodenal cells. Therefore, we decided to corroborate our findings on particle uptake by testing if infectious EAdV entry was clathrin- and actin-dependent.

Consequently, we established an infection setup optimized for cell survival and stable EAdV hexon readout. Due to the slow infection life cycle of EAdV, stable hexon signal was not detectable before 44-48 h post infection. We treated HuTu80 and A549 cells with pitstop2 and cytoD for 30 min before addition of AdV40 or AdV41. The cells were then incubated for 2 h at 37°C until the inoculum was exchanged for medium containing inhibitor. The inhibitor was removed at 24 h post infection to increase cell viability within the assay and cells were fixed and stained for viral hexon and nuclei at 48 h post infection. Interestingly, pitstop2 reduced EAdV infection of HuTu80 and A549 cells only at the highest inhibitor concentration, but not in a dose-dependent manner (Fig. 5B/C). At 5 µM pitstop2, infection of both cell lines with AdV40 and AdV41 was reduced by more than 50% compared to the DMSO treated control. In contrast, cytoD treatment efficiently and dose-dependently reduced infection to about 25% residual infection at the highest drug concentration for HuTu80 and 50% residual infection for A549 (Fig. 5D/E). From these data we conclude that not only overall particle uptake but also infectious EAdV uptake in HuTu80 was clathrin- and actin-dependent.

Figure 5: Infectious internalization of EAdV depends on clathrin in HuTu80 cells. A) Scheme of the infectious internalization assay in presence of inhibitors. B-E) Infectious internalization in the presence of pitstop2 (B/C), cytochalasin D (D/E) in A549 (black) and HuTu80 (red) cells. Infectious internalization after treatment of cells with siRNA against clathrin adapter AP2 or non-targeting siRNA scrambled control. Error bars indicate the standard error of the mean. Statistical significance determined using two-way ANOVA test: *: $p<0.05$, **: $p<0.01$, ***: $p<0.001$, ****: $p<0.0001$.

bioRxiv preprint doi: https://doi.org/10.1101/2023.03.06.531250; this version posted March 6, 2023. The copyright holder for this preprint (which was not certified by peer review) is the author/funder, who has granted bioRxiv a license to display the preprint in perpetuity. It is made available under aCC-BY 4.0 International license.

To verify our findings omitting pitstop2, we used RNA interference against AP2, a clathrin adapter at the plasma membrane (37), followed by infection with EAdV. To generate an efficient knock-down level, we depleted AP2 in HuTu80 and A549 cells by double transfection with 48 h in between with siRNA against AP2 or with a scrambled control (38). We seeded cells 24 h after the second siRNA treatment, infected them 24 h later as stated above and fixed and stained for hexon protein and nuclei at 48 h post infection. We harvested additional cells at the time of infection to determine knock down efficiencies on protein level. Knock down of AP2 reduced infection of HuTu80 by 75% for AdV40 and 40% for AdV41 and infection of A549 by 75% for AdV40 and 50% for AdV41 (Fig. 5F/G). Infection of A549 cells appears to be clathrin- and actin -dependent despite an independence of EAdV overall uptake in presence of pitstop2 (Fig. 4A). This suggests additional clathrin-independent non-productive uptake pathways in A549 cells. In contrast, our uptake and infection assays for HuTu80 consistently suggest a role for CME in EAdV infection. Taken together, we conclude that EAdV can rapidly infect duodenal HuTu80 cells in a clathrin- and actin-dependent manner.

Discussion

In this study, we aimed to evaluate the infectious pathway of EAdVs in duodenal HuTu80 compared to lung-derived A549 cells. Our results show that EAdVs have a kinetic advantage when infecting duodenal cells over lung-derived cells. Furthermore, we find that EAdV enter cells via a clathrin-dependent mechanism in A549 and HuTu80 cells, while clathrin-independent uptake was described for HEK293 cells. A faster and possibly more efficient uptake in HuTu80 cells is well in line with EAdV's natural tropism in the gastrointestinal tract. Differential host cell requirements in uptake pathways and their translational implications have recently become obvious. For example, SARS-CoV-2 enters Vero cells by endocytosis and lung epithelial cells by fusion at the plasma membrane. Thus chloroquine has antiviral effects

bioRxiv preprint doi: https://doi.org/10.1101/2023.03.06.531250; this version posted March 6, 2023. The copyright holder for this preprint (which was not certified by peer review) is the author/funder, who has granted bioRxiv a license to display the preprint in perpetuity. It is made available under aCC-BY 4.0 International license.

365 against SARS-CoV-2 in Vero cells, but not in cells of lung tissue origin (39). This underlines
366 that infection models reflecting the target tissue are vitally important to understand
367 mechanisms of virus entry and infection and to device strategies for antiviral treatment.

368 Historically, EAdV were fastidious and difficult to grow to high infectious titer in tissue
369 cultures (8,9). Even to date, we observe that overall yields and infectious-to-non-infectious
370 particle ratios are poorer than for other adenoviruses (e.g., AdV5 or AdV-D types) (unpublished
371 results, Arnberg Lab, compare S1 Fig.). Despite their relevance as a leading cause of acute
372 infant gastroenteritis (4), EAdV remain understudied (40). EAdVs are found in stool samples
373 from children with acute gastroenteritis but we lack knowledge on their initial target cells or
374 target regions in the gastrointestinal tract. Hence, virus entry studies originate from easily
375 accessible cell lines like A549 and HEK293 cells. In these studies, EAdV uptake into A549
376 cells was slow, and a major fraction of particles were still neutralized by antibodies after 4 h
377 (20). Similarly, AdV41 entry into HEK293 was inefficient (21). These important observations
378 prompted us to study EAdV host factors in cells originating from the gastrointestinal tract. Our
379 results show a faster uptake of EAdVs into HuTu80 cells when directly compared to A549 cells.
380 As the gastrointestinal tract is specialized on nutrient resorption, it is tempting to speculate that
381 the kinetic advantage lies in a different overall endocytic activity in HuTu80 cells. It is, therefore,
382 critical to discriminate between productive and unproductive endocytic uptake of virus
383 particles. To this end we not only compared global virus uptake but also uptake resulting in
384 successful delivery of the virus DNA to the nucleus (i.e., infection). Consistently, we found a
385 faster productive uptake of EAdVs in HuTu80 cells as compared to A549 cells, but no
386 enhanced uptake kinetics for AdV5. This suggests that the infectious route of EAdVs rather
387 than overall endocytic activity was enhanced in HuTu80 cells.

388 We hypothesized that the observed difference in internalization behavior between A549
389 and HuTu80 cells may result from cell-type-dependent surface interactions and/or differential
390 availability of surface receptors, which could in turn affect particle mobility at the cell surface.
391 For this reason, we tracked particles on the cell surface and analyzed their trajectories. We
392 performed single particle tracking of EAdVs and AdV5 on HuTu80 and A549 at early time

bioRxiv preprint doi: https://doi.org/10.1101/2023.03.06.531250; this version posted March 6, 2023. The copyright holder for this preprint (which was not certified by peer review) is the author/funder, who has granted bioRxiv a license to display the preprint in perpetuity. It is made available under aCC-BY 4.0 International license.

393 points after binding, when we suspected most particles to be on the cell surface based on our
394 uptake and infectious internalization kinetics (Fig. 1). We found high variability in the measured
395 diffusion coefficient for all conditions and motion types. We speculate that the variability arises
396 from the multiple possible interactions that occur between AdVs and the cell surface. Strong
397 multivalent interactions between cellular receptors and particle fiber proteins may cause
398 immobile or slow diffusing confined particles, as it would be the case with particles in endocytic
399 pits but also during interaction with attachment factors like heparan sulfate proteoglycans
400 (HSPGs) after initial binding. Higher mobility of particles can arise from binding to mobile
401 receptors on the cell membrane, either displaying free or confined diffusion, or being coupled
402 with the underlying moving matrix. The latter coupling results in directed motion, as suggested
403 for AdV2 in human embryonic retinoblast (HER) 911 cells (16). Matrix coupled motion was
404 observed to be actin-dependent for other viruses (41–43) or even in a microtubule-assisted
405 manner the C-type lectin DC-SIGN in dendritic cells (44). In addition, our method, although
406 confining the observation to few hundreds of nanometers across the apical membrane of the
407 cell, does not allow to distinguish between external and internalized particles. Thus, a small
408 part of the observed motion is likely to be attributed to the movement of endosomes containing
409 viral particles in the proximity of the membrane. We analysed the overall motion behaviour of
410 each particle by developing the “average motion coefficient” (AMC). Here, we found that a
411 higher fraction of the particle population showed a higher mobility with regards to surface
412 explored (AMC score of 2). It is tempting to speculate that the greater fraction of mobile
413 particles reflects viruses bound to mobile receptor species possibly scouting the surface for
414 their site of internalization comparable to faster diffusion of AdV2 interacting with its receptor
415 CAR prior to endocytic uptake (16). EAdV interact with their long fiber with CAR in Chinese
416 hamster ovary cells expressing human CAR (14) and show affinity to HSPGs likely through
417 their short fiber protein as confirmed in surface plasmon resonance measurements with
418 purified fiber knobs (13). In addition, AdV41 penton base can engage laminin-binding integrins
419 as co-receptors in human colon cancer cells (17), however, cell entry competent receptor
420 interactions on A549 or intestinal cells remain unknown. In light of this and taking into account

bioRxiv preprint doi: https://doi.org/10.1101/2023.03.06.531250; this version posted March 6, 2023. The copyright holder for this preprint (which was not certified by peer review) is the author/funder, who has granted bioRxiv a license to display the preprint in perpetuity. It is made available under aCC-BY 4.0 International license.

that HuTu80 cells carry less HSPGs but slightly more CAR on their cell surface than A549 cells (data not shown), EAdV may be slowed by multivalent interactions with HSPGs on A549 and have a surface sampling advantage leading to faster internalization in HuTu80 cells. This hypothesis is also supported by the finding that large extracellular domains, like HSPGs, have smaller diffusion coefficients on giant luminal vesicles (45). To validate this hypothesis, virus particles with short or long fibers only, would be valuable tools to assess the contribution of known receptors to the entry kinetics and diffusion behaviour. Studying surface interactions of EAdV on the two cell lines may also reveal cell type or tissue specific receptors that explain differences in the kinetic behaviours.

EAdVs enter the intestine by passing through the stomach with a low pH milieu. Previous studies demonstrated that EAdV particles are resistant to low pH explaining in part their tropism (18). In our study, we established a low pH wash protocol to block EAdV entry into intestinal epithelial cells. While this seems counterintuitive, we could reproducibly show that cell-bound EAdV particles become non-infectious upon low pH wash. We conclude that EAdV-cell surface molecule interactions induce a conformational change in the EAdV capsid, that renders the virus particles acid sensitive. This is in line with a sequence of entry cues for EAdV as seen for AdV2 in a step-wise process (16,46), starting with attachment to host factors followed by secondary low pH priming in endosomes, which then triggers endosomal membrane rupture and escape. Future work will address whether such sequential entry cues govern EAdV entry into the intestinal epithelium.

Here, we report the first TEM imaging of EAdV particles entering cells of physiological tissue origin. In TEM, EAdV increasingly localized to intracellular compartments (endosomal structures and cytosol) in both cell lines over time reflecting successful virus entry and endosomal escape. The effect was again more pronounced in HuTu80 cells and strongest after 2 h of internalization. This was in line with the effects seen in the early phases (0 – 6 hpi) in the infectious internalization kinetics and supporting the kinetic advantage observed. Virus particles were mainly observed on smooth membranes and membrane invaginations lacking a visible clathrin coat structure indicating a non-clathrin dependent entry pathway. We

bioRxiv preprint doi: https://doi.org/10.1101/2023.03.06.531250; this version posted March 6, 2023. The copyright holder for this preprint (which was not certified by peer review) is the author/funder, who has granted bioRxiv a license to display the preprint in perpetuity. It is made available under aCC-BY 4.0 International license.

449 demonstrated, however, that productive virus uptake and infection was clathrin-dependent in
450 inhibition and RNAi assays. This can be explained by EAdV's slow and protracted entry, where
451 single virus entry events likely occur asynchronously and over an extended period of time as
452 seen for other viruses e.g. Human Papillomavirus 16 (47). In contrast, CME is a fast process,
453 which occurs within 2 min (48). In our assays, we are therefore observing single internalization
454 events at any time point rather than a synchronous entry of many particles. Those events
455 themselves may be fast as they occur by CME. In static experiments like TEM, where we are
456 observing cells at a fixed time point, we hypothesize that we likely miss most endocytic events.
457 We observed a small fraction of viruses in endocytic pits mostly without a clathrin coat, which
458 could indicate that those endocytic events are mechanistically slower or possibly delayed due
459 to inefficient cargo recognition. Orthogonal methods including pharmacological perturbation
460 and RNA interference are clearly better suited to reveal involvement of fast uptake
461 mechanisms. Nonetheless, our TEM analysis confirms a faster uptake of EAdVs into cells of
462 intestinal origin and our data collectively argues for including intestinal epithelial cell lines in
463 the toolbox of EAdV studies.

464 Our pharmacological perturbation and RNA interference studies reveal clathrin-
465 mediated endocytosis as the major entry pathway of EAdVs into intestinal cells. This is in
466 contrast to previous studies on HEK cells (21) and to our observations in A549 cells,
467 highlighting the importance of choice of experimental system. The effects during infectious
468 internalization experiments with pitstop2 only showed a partial effect at the highest inhibitor
469 concentration. Due to high cytotoxicity and possible off-target effects, the drug was washed
470 out after half of the incubation time. This may be the reason for a lack of dose-dependency for
471 pitstop2, as successful entry and hexon production may be possible after wash-out of the drug.
472 Because of these limitations and the debatable specificity of pitstop2 (49,50), we additionally
473 confirmed importance of CME for EAdV entry by RNA interference with the clathrin adapter
474 AP2. Taken together, through orthogonal assays we demonstrated an important role of CME
475 in productive EAdV entry into intestinal epithelial cells. As the cell system used is derived from

bioRxiv preprint doi: https://doi.org/10.1101/2023.03.06.531250; this version posted March 6, 2023. The copyright holder for this preprint (which was not certified by peer review) is the author/funder, who has granted bioRxiv a license to display the preprint in perpetuity. It is made available under aCC-BY 4.0 International license.

tissue of EAdV tropism, we propose that CME is a physiological uptake route. Studies using human intestinal organoids need to confirm this notion.

Our study highlights the importance of studying host factors and infection pathways in appropriate model systems. In contrast to previously used respiratory epithelial cell models, EAdV infection of duodenal HuTu80 cells revealed that EAdV entry is clathrin-dependent and that enhanced infection kinetics may be a measure for infection efficacy. Clearly, cell lines from different tissue backgrounds will remain an important tool to identify and validate host factors during virus infections. This study characterizes duodenal cells as a novel tool for the study of EAdV and reveals previously neglected aspects of the cell entry mechanisms of these medically relevant viruses.

Materials and Methods

Cells, media, chemicals: A549 and HuTu80 cells cultured in DMEM (Sigma, #D5648) supplemented with 1x pen-strep (Gibco, #15140122) and 20 mM HEPES (Thermo Fisher Scientific, #BP310-500) (DPH) and 10% FBS (Hyclone, #SV30160.03) at 37°C and 5% CO_2. For infections medium without FBS was used for incubation (DPH) and changed to medium with low FBS until fixation (DPH + 2% FBS). Small molecule inhibitors were pitstop2 (Abcam, #ab120687), dynasore (Abcam, #ab120192), cytochalasinD (Abcam, #ab143484), methyl-β-cyclodextrin (Sigma, C4555-1G). CsCl was from Sigma (C4036).

Viruses: AdV-F40 (strain Hovix), AdV-F41 (strain Tak), and AdV-C5 (strain adenoid 75) were produced in A549 cells and purified as described previously (51). In brief, detached cells were pelleted at 800 rpm, supernatants were discarded, and cell pellets were suspended in DMEM. For cell lysis and virus extraction, cell suspensions were supplemented with an equal volume of Vertrel XF (Sigma; #94884) and shaken thoroughly. Phases were separated by centrifugation for 10 min at 3000 rpm. The upper aqueous phase was loaded onto a CsCl step

bioRxiv preprint doi: https://doi.org/10.1101/2023.03.06.531250; this version posted March 6, 2023. The copyright holder for this preprint (which was not certified by peer review) is the author/funder, who has granted bioRxiv a license to display the preprint in perpetuity. It is made available under aCC-BY 4.0 International license.

gradient with the densities 1.27, 1.32, and 1.37 (bottom to top) for ultracentrifugation in a SW40 rotor (Beckman Coulter) for 2.5 h at 4°C and 25000 rpm. The virus containing band was extracted from the gradient and desalted on a NAP column (VWR, Cytiva, Illustra NAP) by elution in PBS, pH 7.4 and frozen at -80°C after addition of 10% glycerol.

AF488-labeled AdV: AdV stocks were produced as above and used frozen (AdV5) or fresh (AdV40 and AdV41) for covalent labeling with AF488-NHS (Thermo Fisher Scientific; #A20000). Viruses were used at a concentration of at least 500 ng/µL (best 1000 ng/µL) and incubated with 10-fold molar excess dye over virus in a 500 µL reaction for 1 h rotating and light protected at room temperature. Virus was separated from free dye by ultracentrifugation as above on a SW60Ti rotor (Beckman Coulter). The virus band was extracted and desalted on a NAP column (VWR, Cytiva, Illustra NAP) by elution in PBS, pH 7.4 and frozen in small aliquots at -80°C after addition of 4% glycerol.

Immunofluorescence staining: 75000 A549 cells were seeded in growth medium on ibidi 8-well µ-slides (ibidi, #80826) 24 h prior to experimentation. AF488-labeled AdVs were bound to cells at 4°C on ice for 1 h. Medium was exchanged, and cells were either kept at 4°C or shifted to 37°C for 4 h for internalization. Samples were transferred to 4°C for staining with anti-AF488-antibody (rabbit, Thermo Fisher Scientific; #A-11094) for 30 min on ice shaking, washed once with cold PBS + 2% FBS and subsequently stained with anti-rabbit IgG-AF568 for 30 min at 4°C shaking. Cells were fixed with 4% PFA/PBS for 20 min and stained with AF647-Wheat Germ Agglutinin (WGA, Thermo Fisher Scientific, # W32466) and Hoechst33342 (Thermo Fisher Scientific; #62249). Samples were imaged as z-stacks with a 63x objective on a Leica SP8 confocal microscope at the Biochemical Imaging Center Umeå (BICU). Images were processed by maximum intensity projection with Fiji (52).

Uptake assay: Cells were detached with PBS/EDTA, pelleted, suspended in DPH + 10% FBS and kept in suspension on a shaker for 1 h for recovery. $2x10^5$ cells/well were pelleted in a v-bottom 96-well plate and washed with cold DPH. For uptake assays in presence of inhibitors, cells were preincubated with inhibitor dilutions in DPH for 30 min before subsequent virus

bioRxiv preprint doi: https://doi.org/10.1101/2023.03.06.531250; this version posted March 6, 2023. The copyright holder for this preprint (which was not certified by peer review) is the author/funder, who has granted bioRxiv a license to display the preprint in perpetuity. It is made available under aCC-BY 4.0 International license.

incubation. Cells were resuspended in 100 µL DPH (with or without inhibitors) containing AF488-labeled viruses and incubated on ice for 1 h. Cells were pelleted and washed once with 100 µL cold DPH. Control samples were left on ice and internalization samples were transferred to 37°C for 4 h. Cells were pelleted and incubated with anti-AF488-antibody (rabbit, Thermo Fisher Scientific; #A-11094) for 30 min on ice shaking, washed once with cold PBS + 2% FBS and subsequently incubated with anti-rabbit IgG-AF568 for 30 min at 4°C shaking. Cells were washed once with cold PBS + 2% FBS and resuspended in 50 µL cold PBS + 2% FBS. Samples were measured by flow cytometry (BD Accuri) to assess mean fluorescence intensities of AF488 and AF568.

Infectious entry assay: 25000 A549 or 30000 HuTu80 cells per well were seeded in a black optical bottom 96-well plate (Greiner Bio-one; #655096) 24 h prior to experimentation. *Titration:* Virus stocks were titrated for every batch to determine a dilution that results in 20% absolute infection. Virus stocks were diluted serially in DPH, 50 µL of the virus dilution was added to cells and incubated for 2 h at 37°C. Inoculum was removed, samples were supplemented with DPH + 2% FBS, and incubated until 48 hpi. Cells were fixed by addition of 8% paraformaldehyde in PBS to the culture medium and incubated at room temperature for 15 min. *pH-wash:* pH sensitivity of EAdV infection after cell surface binding was tested by a 2 min pH wash after virus binding in DPH for 1 h on ice. Cells were incubated for 2 min with either 0.1 M citrate/PBS buffer (pH 3-6) or 0.1 M CAPS/PBS (pH 8-11) or PBS (pH 7.4). Samples were neutralized by two washes with PBS and subsequent addition of DPH + 2% FBS until fixation with 8% paraformaldehyde in PBS at 48 h post infection. *Kinetics:* Cells were washed once with DPH without FBS and transferred to 4°C. Medium was removed and 50 µL virus dilution was added to each well for binding at 4°C for 2 h. Inoculum was removed and warm DPH + 2% FBS was added to each well. At each time point, duplicate samples were washed with 0.1 M citrate buffer pH 3 for 2 min, subsequently washed gently with PBS and supplemented with warm DPH + 2% FBS until fixation with 4% paraformaldehyde in PBS at 48 h post infection. *Inhibitor:* Cells were incubated with inhibitors dilutions in DPH for 30 min at 37°C. Meanwhile, virus dilutions were mixed with the inhibitors dilutions in a dilution plate.

bioRxiv preprint doi: https://doi.org/10.1101/2023.03.06.531250; this version posted March 6, 2023. The copyright holder for this preprint (which was not certified by peer review) is the author/funder, who has granted bioRxiv a license to display the preprint in perpetuity. It is made available under aCC-BY 4.0 International license.

Medium was removed from the cells and 50 µL virus-inhibitor dilution was added to each well for initial binding and internalization for 2 h at 37°C. Then, inoculum was removed and 100 µL inhibitor dilutions mixed with DPH + 4% FBS was added to each well for 24 h. Thereafter, medium was removed and 100 µL warm DPH + 2% FBS was added until fixation with 4% paraformaldehyde in PBS at 48 h post infection. *Staining:* Cells were permeabilized with 100% ice-cold methanol for 20 min at -20°C and rehydrated by washing with PBS and then stained for viral hexon protein expression with an anti-hexon primary antibody (mouse; Merck; #MAB8052) and an anti-mouse secondary antibody coupled to AF488 or AF647 (Thermo Fisher Scientific; #A-11001/#A-21235). Nuclei were stained with Hoechst33342 (Thermo Fisher Scientific; #62249) and used to determine cell numbers. Plates were scanned in a Biotek Cytation5 automated microscope with a 10x objective with subsequent image analysis for cell count and infection counting or using the Tina program a TROPHOS plate reader (Luminy Biotech Enterprises, Marseille, France).

SiRNA knockdown: 250000 A549 or 350000 HuTu80 cells per well were seeded in 12-well plates 24 h prior to experimentation. Cells were transfected with 15 nM siRNA (AP2M1: Thermo Fisher Scientific # 1299001, HSS101955; SCR: Thermo Fisher Scientific #12935300) with 3.33 µL Lipofectamine RNAiMax (Thermo Fisher Scientific, #13778075) following the recommended protocol. The transfection mixture was added dropwise to wells containing 1 mL DPH + 10% FBS and not removed until next day. Cells were split into a 6-well plate on the next day. Cells were transfected with 5 nM siRNA (A549) or 15 nM siRNA (HuTu80) with 5 µL Lipofectamine RNAiMax following the recommended protocol. The transfection mixture was added dropwise to wells containing 2 mL DPH + 10% FBS and kept until next day. Cells were seeded into 96 well plates for infection experiment as described above and into 48 or 24 well plates for Western Blot. Cells were harvested for Western Blotting by addition of 2x loading dye/DTT. Samples were boiled for 10 min and frozen at -20°C. Samples were separated on precast gel (4-12% NuPAGE Bis-Tris, Thermo Fisher Scientific, #NP0321BOX) with 1x MOPS buffer (Novex, NuPage, #NP0001) for 1 h at 100 V. Proteins were transferred to a nitrocellulose membrane (0.2 µm, BioRad, #162-0112) with transfer buffer (20% methanol, 39 mM glycine,

bioRxiv preprint doi: https://doi.org/10.1101/2023.03.06.531250; this version posted March 6, 2023. The copyright holder for this preprint (which was not certified by peer review) is the author/funder, who has granted bioRxiv a license to display the preprint in perpetuity. It is made available under aCC-BY 4.0 International license.

48 mM Tris base, 0.037% SDS) for 75 min at 100 V. Membranes were blocked with 2% ECL prime blocking reagent in PBS-T (Amersham; #RPN418) and incubated against AP-2 (mouse-anti-AP50, BD, #A611351) and GAPDH (rabbit-anti-GAPDH, Sigma, #G9545-100uL) in blocking buffer over night at 4°C. Signals were detected by chemiluminescence using anti-mouse/rabbit-HRP secondary antibodies (Novex, A16072/A16104) and ECL substrates (Thermo Fisher Scientific, #34577/34095). Membranes were imaged on an Amersham imager 680 (GE/Cytiva).

Transmission electron microscopy: $1x10^6$ A549 and HuTu80 cells per well were seeded in a 6-well plate on the day prior to experimentation. Cells were transferred to ice and washed twice with cold DPH. Viruses were diluted at 50000 particles per cell (based on 11 ng virus preparation contains $4x10^7$ particles (53)) and added to cells on ice. Samples were incubated on ice for binding for 1 h shaking. Thereafter, virus inoculum was removed and warm DPH + 2% FBS was added to each well. Samples were transferred to 37°C and internalization was allowed for 12.5 min, 2 h and 6 h. After incubation, medium was removed and 1.5 mL EM-fixative (2.5% glutaraldehyde, 0.05% malachite green, 0.1 M phosphate buffer (PB; NaH_2PO_4 + MQ-water) (Taab Laboratory Equipment Ltd, Aldermaston, UK). for 1 h at room temperature. Fixed samples were washed twice with 2 mL 0.1 M PB and kept in 0.1 M PB until processing. All the below chemical fixation steps were performed in the microwave Pelco biowave pro+ (Ted Pella, Redding, CA) unless stated. The samples were rinsed 2x with PB and post-fixed with 0.8% $K_3Fe(CN)_6$ and 1% OsO_4 in 0.1 M PB for 14 min and were rinsed 2x with MQ-water. The samples were then stained with 1% aqueous tannic acid. Following 2x rinse in MQ-water, samples were stained with 1% aqueous uranyl acetate (Polysciences, Inc., Hirschberg an der Bergstrasse, DE). After 2x MQ-water rinses, samples were dehydrated in gradients of ethanol (30%, 50%, 70%, 80%, 90%, 95%, 100% and 100%). The samples were infiltrated with graded series of Spurr resin in ethanol (1:3, 1:1 and 3:1). After microwave, samples were infiltrated twice with 100% resin before polymerization overnight at 60°C. Samples were sectioned (70 nm) and imaged with Talos 120C (FEI, Eindhoven, The Netherlands) operating at 120 kV at

bioRxiv preprint doi: https://doi.org/10.1101/2023.03.06.531250; this version posted March 6, 2023. The copyright holder for this preprint (which was not certified by peer review) is the author/funder, who has granted bioRxiv a license to display the preprint in perpetuity. It is made available under aCC-BY 4.0 International license.

612 the Umeå Core Facility for Electron Microscopy (UCEM). Micrographs were acquired with a
613 Ceta 16M CCD camera (FEI, Eindhoven, The Netherlands).

614 **Diffusion measurement:** Imaging of AdV particles diffusing on live cells was performed using
615 a Nikon Ti2-E inverted microscope equipped with a two-color laser source (wavelengths: 488
616 nm and 562 nm), a Prime 95B sCMOS camera (Teledyne Photometrics) and a multiband filter
617 cube (86012v2 DAPI/FITC/TxRed/Cy5, Nikon Corp.). The images were collected using a 60x
618 oil immersion objective (numerical aperture: 1.49, MRD01691, Nikon Corp.), 488 nm excitation
619 wavelength and HILO microscopy configuration, which allows imaging of the apical cell surface
620 while reducing out-of-focus signal and background noise when compared to epifluorescence.
621 For the experiments, 40000 A549 and 50000 HuTu80 cells per well were seeded in a glass-
622 bottom 96-well plate 24 h before imaging. The following day, the culture medium was removed
623 and replaced with warm DMEM without phenol red and 2% FBS to reduce the background
624 signal in fluorescence imaging. Cells were incubated at 37°C for 1 h and, right before the
625 experiment, the plate was transferred under the microscope and kept at 37°C and 100%
626 humidity in a dedicated on-stage incubator (Okolab). 100 µl of AF488 labelled AdV in a
627 premixed 1:50 dilution was added in each well, pipetting thoroughly to homogenize the virus
628 particle distribution in the cell medium. After 5 min, the cell supernatant was removed, and the
629 well was washed twice with fresh prewarmed medium. Cells were imaged 5 and 30 minutes
630 after washing. Videos were acquired at 10 frames per second for 2 min. Two videos were
631 acquired for the 5 min and between 2 and 4 videos for the 30 min time point. The frame rate
632 was optimized to guarantee good time resolution and a high signal-to-noise ratio. All conditions
633 were acquired in duplicates.

634 **Single particle tracking and diffusion analysis**: The recorded time-lapses were processed
635 to remove the background and improve contrast with an in-house ImageJ script. First, a
636 Gaussian filter with a sigma of 0.5 pixels was convolved to the image to reduce the camera
637 noise. Bleaching was then corrected using a built-in Fiji function, which fits the variation of total
638 intensity in time to an exponential fit (52). The background signal was calculated by averaging

bioRxiv preprint doi: https://doi.org/10.1101/2023.03.06.531250; this version posted March 6, 2023. The copyright holder for this preprint (which was not certified by peer review) is the author/funder, who has granted bioRxiv a license to display the preprint in perpetuity. It is made available under aCC-BY 4.0 International license.

over all the frames and then applying a Gaussian filter with a sigma of 20 pixels. This removes the fine details, like immobile viruses, while maintaining the broader cellular features. The background was then subtracted from each frame. The virus particles were then detected and tracked using the Laplacian Gaussian filter in the TrackMate plugin, which allows for sub-pixel resolution on the particle position (54). Linking between frames is performed using a maximum linking displacement of 1 µm, and a maximum frame gap of 10. The obtained trajectories were segmented according to the characteristics of the motion displayed using a DC-MSS algorithm (24), and each segment was assigned to a motion type, according to the slope of the moment scaling spectrum. The motion type considered were immobile, confined motion, free diffusion and directed motion. In-house scripts were used to extract diffusion parameters, e.g. Diffusion coefficient (D) and confinement radius (R_C), of both each segment and each unsegmented track. Only tracks with a duration of more than 300 frames (30 seconds) were considered in the analysis of unsegmented tracks. The tracks were classified considering the average time spent in each motion type. A numerical value was assigned to each motion type (0: immobile, 1: confined motion, 2: free diffusion, 3: directed motion) and the weighted average over the time spent in each motion type was calculated resulting in a numerical coefficient (“average motion coefficient”) between 0 (fully immobile) and 3 (only directed motion). A value of 1.5 was considered as the threshold between particles dominated by confined diffusion and particles displaying mostly free or directed motion.

Acknowledgements

We acknowledge the Biochemical Imaging Center and Umeå Core Facility for Electron Microscopy at Umeå University and the National Microscopy Infrastructure, NMI (VR-RFI 2019-00217) for providing assistance in microscopy.

bioRxiv preprint doi: https://doi.org/10.1101/2023.03.06.531250; this version posted March 6, 2023. The copyright holder for this preprint (which was not certified by peer review) is the author/funder, who has granted bioRxiv a license to display the preprint in perpetuity. It is made available under aCC-BY 4.0 International license.

References

1. Benkő M, Aoki K, Arnberg N, Davison AJ, Echavarría M, Hess M, et al. ICTV Virus Taxonomy Profile: Adenoviridae 2022: This article is part of the ICTV Virus Taxonomy Profiles collection. J Gen Virol [Internet]. 2022 Mar 30 [cited 2023 Jan 10];103(3). Available from: https://www.microbiologyresearch.org/content/journal/jgv/10.1099/jgv.0.001721

2. HAdV Working Group,. Adenovirus repository http://hadvwg.gmu.edu/ [Internet]. [cited 2023 Feb 3]. Available from: http://hadvwg.gmu.edu/

3. Uhnoo I, Wadell G, Svensson L, Johansson ME. Importance of enteric adenoviruses 40 and 41 in acute gastroenteritis in infants and young children. J Clin Microbiol. 1984;20(3):365–72.

4. Liu J, Platts-Mills JA, Juma J, Kabir F, Nkeze J, Okoi C, et al. Use of quantitative molecular diagnostic methods to identify causes of diarrhoea in children: a reanalysis of the GEMS case-control study. The Lancet. 2016;388(10051):1291–301.

5. Troeger C, Blacker BF, Khalil IA, Rao PC, Cao S, Zimsen SR, et al. Estimates of the global, regional, and national morbidity, mortality, and aetiologies of diarrhoea in 195 countries: a systematic analysis for the Global Burden of Disease Study 2016. Lancet Infect Dis. 2018;18(11):1211–28.

6. World Health Organization. Disease Outbreak News; Acute hepatitis of unknown aetiology in children - Multi-country. [Internet]. 2022 [cited 2023 Feb 3]. Available from: https://www.who.int/emergencies/disease-outbreak-news/item/2022-DON400

7. GOV.UK. Acute hepatitis: technical briefing [Internet]. GOV.UK. 2022 [cited 2023 Feb 3]. Available from: https://www.gov.uk/government/publications/acute-hepatitis-technical-briefing

8. Kidd AH, Schoub BD. FASTIDIOUS ADENOVIRUSES. The Lancet. 1982 Jul;320(8288):51.

9. Tiemessen CT, Kidd AH. Adenovirus type 40 and 41 growth in vitro: host range diversity reflected by differences in patterns of DNA replication. J Virol. 1994 Feb;68(2):1239–44.

10. Wilcox WC, Ginsberg HS, Anderson TF. STRUCTURE OF TYPE 5 ADENOVIRUS. J Exp Med. 1963 Aug 1;118(2):307–14.

11. Kidd AH, Chroboczek J, Cusack S, Ruigrok RWH. Adenovirus Type 40 Virions Contain Two Distinct Fibers. Virology. 1993 Jan;192(1):73–84.

12. Hung-Yueh Y, Pieniazek N, Pieniazek D, Gelderblom H, Luftig RB. Human adenovirus type 41 contains two fibers. Virus Res. 1994 Aug;33(2):179–98.

13. Rajan A, Palm E, Trulsson F, Mundigl S, Becker M, Persson BD, et al. Heparan Sulfate Is a Cellular Receptor for Enteric Human Adenoviruses. Viruses. 2021 Feb 14;13(2):298.

bioRxiv preprint doi: https://doi.org/10.1101/2023.03.06.531250; this version posted March 6, 2023. The copyright holder for this preprint (which was not certified by peer review) is the author/funder, who has granted bioRxiv a license to display the preprint in perpetuity. It is made available under aCC-BY 4.0 International license.

14. Roelvink PW, Lizonova A, Lee JGM, Li Y, Bergelson JM, Finberg RW, et al. The Coxsackievirus-Adenovirus Receptor Protein Can Function as a Cellular Attachment Protein for Adenovirus Serotypes from Subgroups A , C , D , E , and F. 1998;72(10):7909–15.

15. Wickham TJ, Mathias P, Cheresh DA, Nemerow GR. Integrins αvβ3 and αvβ5 promote adenovirus internalization but not virus attachment. Cell. 1993 Apr 23;73(2):309–19.

16. Burckhardt CJ, Suomalainen M, Schoenenberger P, Boucke K, Hemmi S, Greber UF. Drifting motions of the adenovirus receptor CAR and immobile integrins initiate virus uncoating and membrane lytic protein exposure. Cell Host Microbe. 2011;10(2):105–17.

17. Rajan A, Persson BD, Frängsmyr L, Olofsson A, Sandblad L, Heino J, et al. Enteric Species F Human Adenoviruses use Laminin-Binding Integrins as Co-Receptors for Infection of Ht-29 Cells. Sci Rep. 2018;8(1):1–14.

18. Favier AL, Burmeister WP, Chroboczek J. Unique physicochemical properties of human enteric Ad41 responsible for its survival and replication in the gastrointestinal tract. Virology. 2004;322(1):93–104.

19. Rafie K, Lenman A, Fuchs J, Rajan A, Arnberg N, Carlson LA. The structure of enteric human adenovirus 41—A leading cause of diarrhea in children. Sci Adv. 2021 Jan 6;7(2).

20. Albinsson B, Kidd AH. Adenovirus type 41 lacks an RGD αv-integrin binding motif on the penton base and undergoes delayed uptake in A549 cells. Virus Res. 1999 Nov;64(2):125–36.

21. Leung TKH, Brown M. Block in entry of enteric adenovirus type 41 in HEK293 cells. Virus Res. 2011;156(1–2):54–63.

22. Holly MK, Smith JG. Adenovirus Infection of Human Enteroids Reveals Interferon Sensitivity and Preferential Infection of Goblet Cells. J Virol. 2018;92(9):1–15.

23. Tokunaga M, Imamoto N, Sakata-Sogawa K. Highly inclined thin illumination enables clear single-molecule imaging in cells. Nat Methods. 2008 Feb;5(2):159–61.

24. Vega AR, Freeman SA, Grinstein S, Jaqaman K. Multistep Track Segmentation and Motion Classification for Transient Mobility Analysis. Biophys J. 2018 Mar;114(5):1018–25.

25. Abidine Y, Liu L, Wallén O, Trybala E, Olofsson S, Bergström T, et al. Cellular Chondroitin Sulfate and the Mucin-like Domain of Viral Glycoprotein C Promote Diffusion of Herpes Simplex Virus 1 While Heparan Sulfate Restricts Mobility. Viruses. 2022 Aug 21;14(8):1836.

26. Kaksonen M, Roux A. Mechanisms of clathrin-mediated endocytosis. Nat Rev Mol Cell Biol. 2018 May;19(5):313–26.

27. Meier O, Boucke K, Hammer SV, Keller S, Stidwill RP, Hemmi S, et al. Adenovirus triggers macropinocytosis and endosomal leakage together with its clathrin-mediated uptake. J Cell Biol. 2002 Sep 16;158(6):1119–31.

bioRxiv preprint doi: https://doi.org/10.1101/2023.03.06.531250; this version posted March 6, 2023. The copyright holder for this preprint (which was not certified by peer review) is the author/funder, who has granted bioRxiv a license to display the preprint in perpetuity. It is made available under aCC-BY 4.0 International license.

737 28. Von Kleist L, Stahlschmidt W, Bulut H, Gromova K, Puchkov D, Robertson MJ, et al.
738 Role of the clathrin terminal domain in regulating coated pit dynamics revealed by small
739 molecule inhibition. Cell. 2011;146(3):471–84.

740 29. Doherty GJ, McMahon HT. Mechanisms of endocytosis. Annu Rev Biochem.
741 2009;78:857–902.

742 30. Kirchhausen T, Macia E, Pelish HE. Use of Dynasore, the Small Molecule Inhibitor of
743 Dynamin, in the Regulation of Endocytosis. In: Methods in Enzymology. Elsevier; 2008.
744 p. 77–93.

745 31. Simons K, Ikonen E. Functional rafts in cell membranes. Nature. 1997
746 Jun;387(6633):569–72.

747 32. Maxfield FR, Tabas I. Role of cholesterol and lipid organization in disease. Nature. 2005
748 Dec 1;438(7068):612–21.

749 33. Klein U, Gimpl G, Fahrenholz F. Alteration of the Myometrial Plasma Membrane
750 Cholesterol Content with .beta.-Cyclodextrin Modulates the Binding Affinity of the
751 Oxytocin Receptor. Biochemistry. 1995 Oct 1;34(42):13784–93.

752 34. Kilsdonk EPC, Yancey PG, Stoudt GW, Bangerter FW, Johnson WJ, Phillips MC, et al.
753 Cellular Cholesterol Efflux Mediated by Cyclodextrins. J Biol Chem. 1995
754 Jul;270(29):17250–6.

755 35. Pollard TD, Cooper JA. Actin, a Central Player in Cell Shape and Movement. Science.
756 2009 Nov 27;326(5957):1208–12.

757 36. Brown SS, Spudich JA. Cytochalasin inhibits the rate of elongation of actin filament
758 fragments. J Cell Biol. 1979;83(3):657–62.

759 37. Robinson MS. Adaptable adaptors for coated vesicles. Trends Cell Biol. 2004
760 Apr;14(4):167–74.

761 38. Motley A, Bright NA, Seaman MNJ, Robinson MS. Clathrin-mediated endocytosis in AP-
762 2–depleted cells. J Cell Biol. 2003 Sep 1;162(5):909–18.

763 39. Hoffmann M, Mösbauer K, Hofmann-Winkler H, Kaul A, Kleine-Weber H, Krüger N, et al.
764 Chloroquine does not inhibit infection of human lung cells with SARS-CoV-2. Nature.
765 2020 Sep 24;585(7826):588–90.

766 40. Lee B, Damon CF, Platts-Mills JA. Pediatric acute gastroenteritis associated with
767 adenovirus 40/41 in low-income and middle-income countries. Curr Opin Infect Dis. 2020
768 Oct;33(5):398–403.

769 41. Schelhaas M, Ewers H, Rajamäki ML, Day PM, Schiller JT, Helenius A. Human
770 papillomavirus type 16 entry: Retrograde cell surface transport along actin-rich
771 protrusions. PLoS Pathog. 2008;4(9).

bioRxiv preprint doi: https://doi.org/10.1101/2023.03.06.531250; this version posted March 6, 2023. The copyright holder for this preprint (which was not certified by peer review) is the author/funder, who has granted bioRxiv a license to display the preprint in perpetuity. It is made available under aCC-BY 4.0 International license.

42. Coller KE, Berger KL, Heaton NS, Cooper JD, Yoon R, Randall G. RNA Interference and Single Particle Tracking Analysis of Hepatitis C Virus Endocytosis. PLOS Pathog. 2009 Dec 24;5(12):e1000702.

43. Burckhardt CJ, Greber UF. Virus movements on the plasma membrane support infection and transmission between cells. PLoS Pathog. 2009;5(11).

44. Liu P, Weinreb V, Ridilla M, Betts L, Patel P, de Silva AM, et al. Rapid, directed transport of DC-SIGN clusters in the plasma membrane. Sci Adv [Internet]. 2017 Nov 8 [cited 2023 Feb 9];3(11). Available from: https://www.science.org/doi/10.1126/sciadv.aao1616

45. Gurdap CO, Wedemann L, Sych T, Sezgin E. Influence of the extracellular domain size on the dynamic behavior of membrane proteins. Biophys J. 2022 Oct 18;121(20):3826–36.

46. Nakano MY, Boucke K, Suomalainen M, Stidwill RP, Greber UF. The First Step of Adenovirus Type 2 Disassembly Occurs at the Cell Surface, Independently of Endocytosis and Escape to the Cytosol. J Virol. 2000 Aug;74(15):7085–95.

47. Becker M, Greune L, Schmidt MA, Schelhaas M. Extracellular Conformational Changes in the Capsid of Human Papillomaviruses Contribute to Asynchronous Uptake into Host Cells. J Virol. 2018;92(11):e02106-17.

48. Cocucci E, Aguet F, Boulant S, Kirchhausen T. The first five seconds in the life of a clathrin-coated pit. Cell. 2012;150(3):495–507.

49. Dutta D, Williamson CD, Cole NB, Donaldson JG. Pitstop 2 Is a Potent Inhibitor of Clathrin-Independent Endocytosis. PLoS ONE. 2012 Sep 21;7(9):e45799.

50. Willox AK, Sahraoui YME, Royle SJ. Non-specificity of Pitstop 2 in clathrin-mediated endocytosis. Biol Open. 2014 Apr 4;3(5):326–31.

51. Mei YF, Lindman K, Wadell G. Two Closely Related Adenovirus Genome Types with Kidney or Respiratory Tract Tropism Differ in Their Binding to Epithelial Cells of Various Origins. Virology. 1998 Jan;240(2):254–66.

52. Schindelin J, Arganda-Carreras I, Frise E, Kaynig V, Longair M, Pietzsch T, et al. Fiji: an open-source platform for biological-image analysis. Nat Methods. 2012 Jul;9(7):676–82.

53. Sweeney JA, Hennessey JP. Evaluation of accuracy and precision of adenovirus absorptivity at 260 nm under conditions of complete DNA disruption. Virology. 2002;295(2):284–8.

54. Tinevez JY, Perry N, Schindelin J, Hoopes GM, Reynolds GD, Laplantine E, et al. TrackMate: An open and extensible platform for single-particle tracking. Methods. 2017 Feb;115:80–90.

bioRxiv preprint doi: https://doi.org/10.1101/2023.03.06.531250; this version posted March 6, 2023. The copyright holder for this preprint (which was not certified by peer review) is the author/funder, who has granted bioRxiv a license to display the preprint in perpetuity. It is made available under aCC-BY 4.0 International license.

Supporting information

S1 Fig. Infection titration A549 and HuTu80. A-C) Susceptibility of A549 (black) and HuTu80 (red) cells to AdV40, AdV41, and AdV5 infection. Shown are typical dilution series and absolute infection values from three independent experiments. Error bars indicate the standard error of the mean.

S2 Fig. Low pH wash after cell binding renders EAdVs non-infectious. A/B) Sensitivity of EAdV infection to low pH wash after binding to A549 cells. Error bars indicate the standard error of the mean. Statistical significance determined using two-way ANOVA test: *: $p<0.05$, **: $p<0.01$, ***: $p<0.001$, ****: $p<0.0001$.

S3 Fig. No clear trend is observed in the diffusion coefficient. Diffusion coefficient of AdVs after 5 and 30 min from the removal of the inoculum and on A549 and HuTu80 cells for (A) confined diffusion, (B) free diffusion and (C) directed motion. Grey dots indicate the mean value for each recorded video. Error bars indicate the standard error of the mean.

S4 Fig. Diffusion regimes segmentation: A) Fraction of the total track time spent in each motion type by AdV particles on A549 and HuTu80 cells after 5 and 30 min from the removal of the inoculum. B/C) Comparison of the total track time spent in immobile (B) and directed (C) diffusion on A549 and HuTu80 cells after 5 and 30 min. Grey dots indicate the value for each recorded video. Error bars indicate the standard error of the mean. Statistical significance determined using two-way ANOVA test: *: $p<0.05$, **: $p<0.01$, ***: $p<0.001$, ****: $p<0.0001$. D) Example track showing how the maximum distance travelled per track segment was calculated. E) Comparison between the fraction of time, of the total length of the track in each segment, and of the maximum distance traveled, i.e., the distance between the two furthest points of each segment, in each motion regime for the track in (D). F) Fraction of the distance travelled in each motion regime for AdV particles on A549 and HuTu80 cells.

bioRxiv preprint doi: https://doi.org/10.1101/2023.03.06.531250; this version posted March 6, 2023. The copyright holder for this preprint (which was not certified by peer review) is the author/funder, who has granted bioRxiv a license to display the preprint in perpetuity. It is made available under aCC-BY 4.0 International license.

832

bioRxiv preprint doi: https://doi.org/10.1101/2023.03.06.531250; this version posted March 6, 2023. The copyright holder for this preprint (which was not certified by peer review) is the author/funder, who has granted bioRxiv a license to display the preprint in perpetuity. It is made available under aCC-BY 4.0 International license.

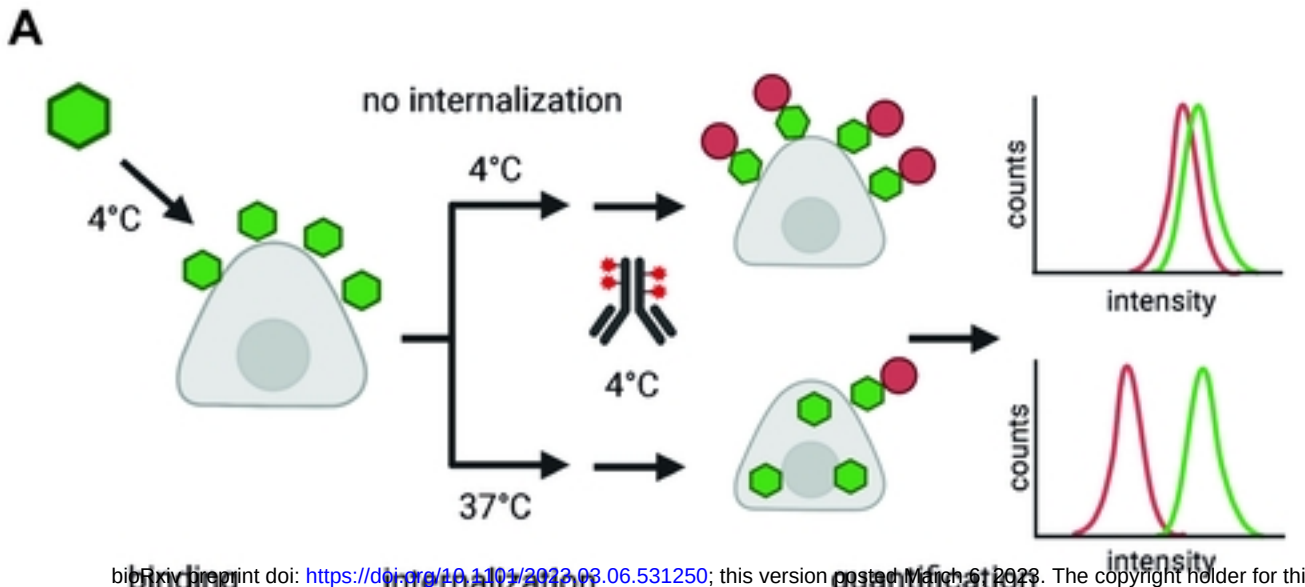

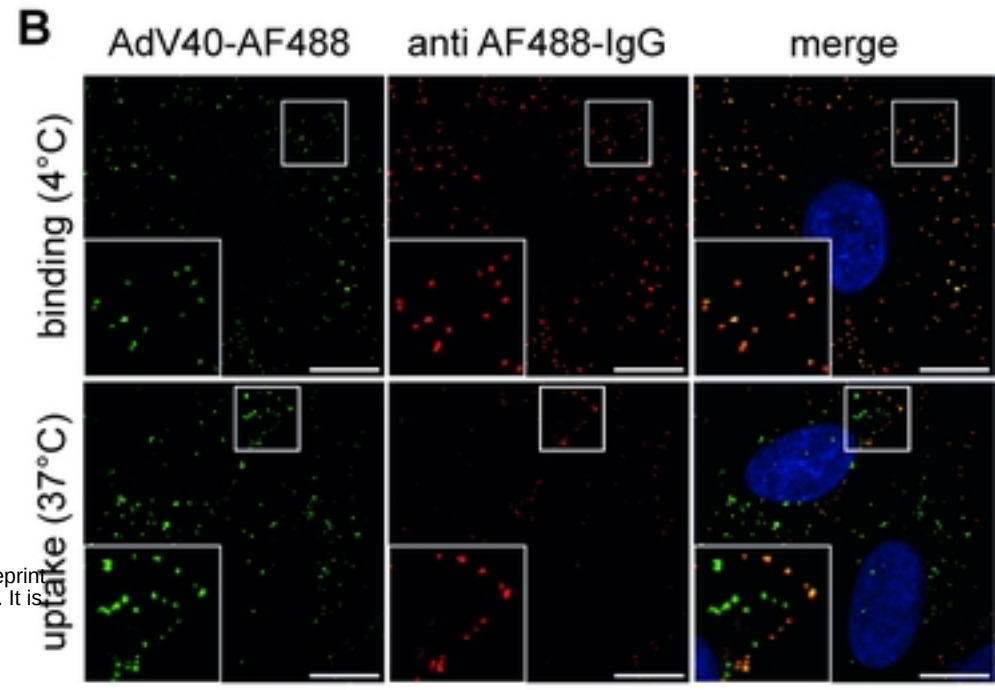

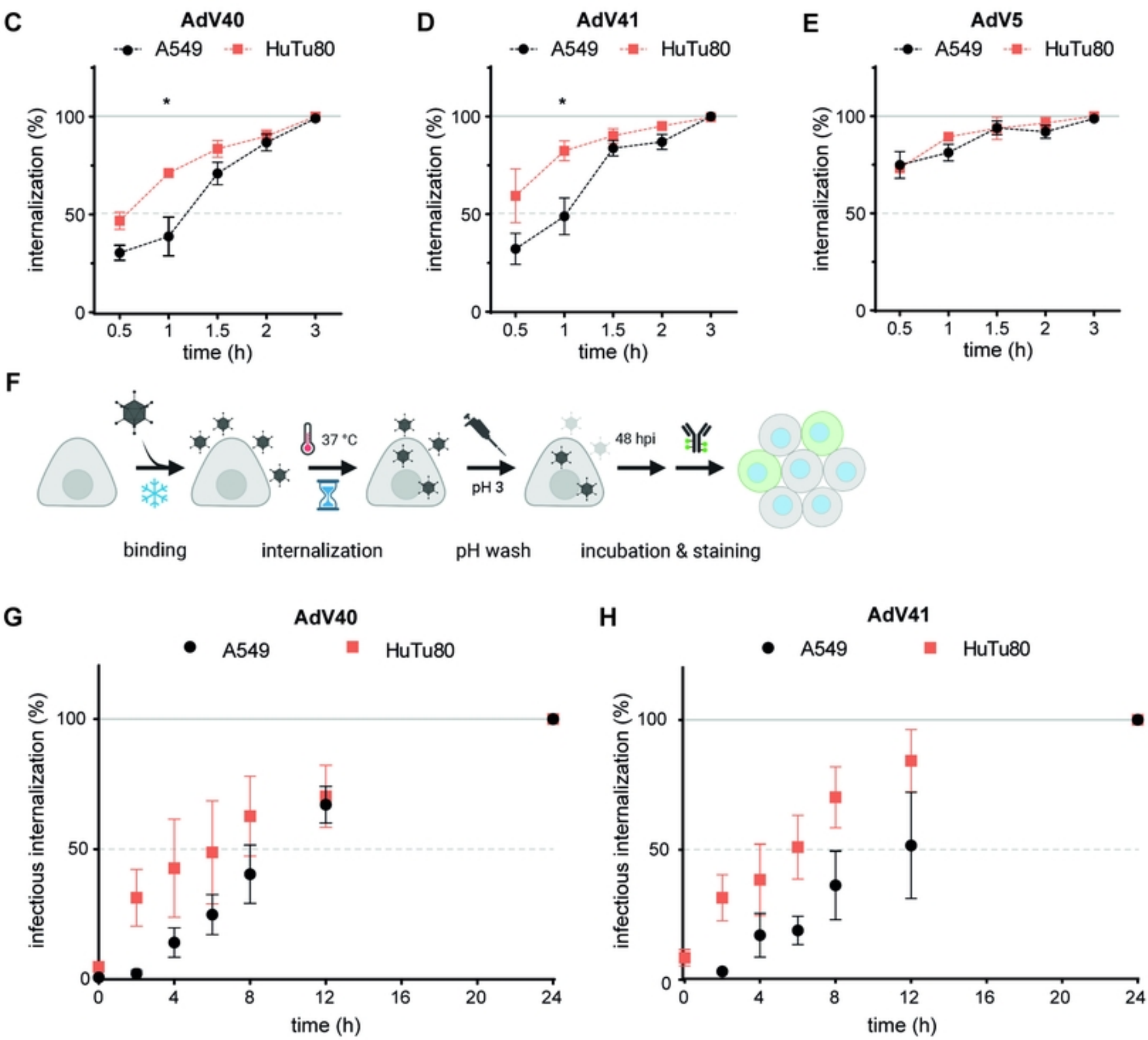

Figure 1

bioRxiv preprint doi: https://doi.org/10.1101/2023.03.06.531250; this version posted March 6, 2023. The copyright holder for this preprint (which was not certified by peer review) is the author/funder, who has granted bioRxiv a license to display the preprint in perpetuity. It is made available under aCC-BY 4.0 International license.

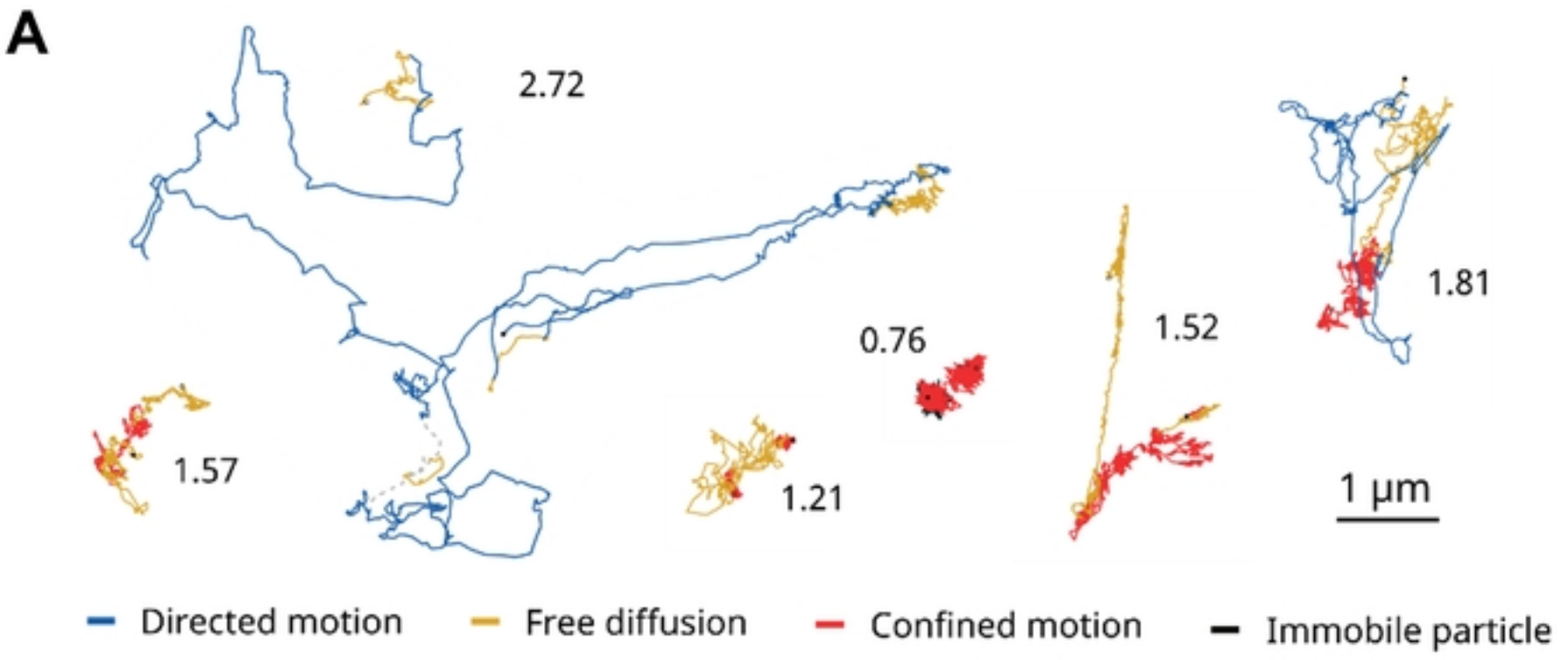

Figure 2

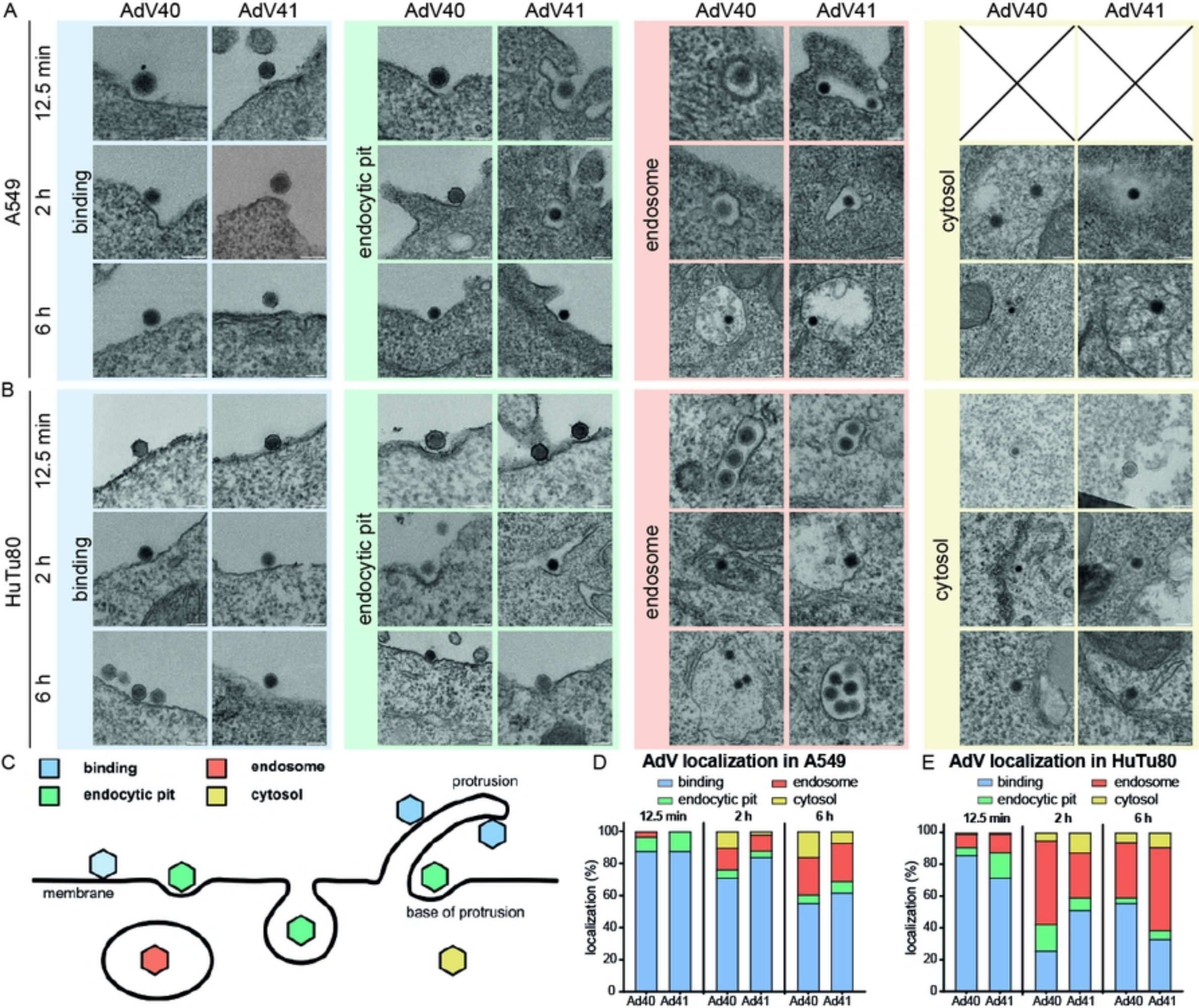
A
AdV40
AdV41
A549
12.5 min
2 h
6 h
binding
endocytic pit
endosome
cytosol
B
HuTu80
C
binding
endocytic pit
endosome
cytosol
protrusion
membrane
base of protrusion
D
AdV localization in A549
localization (%)
12.5 min
2 h
6 h
Ad40
Ad41
E
AdV localization in HuTu80

Figure 3

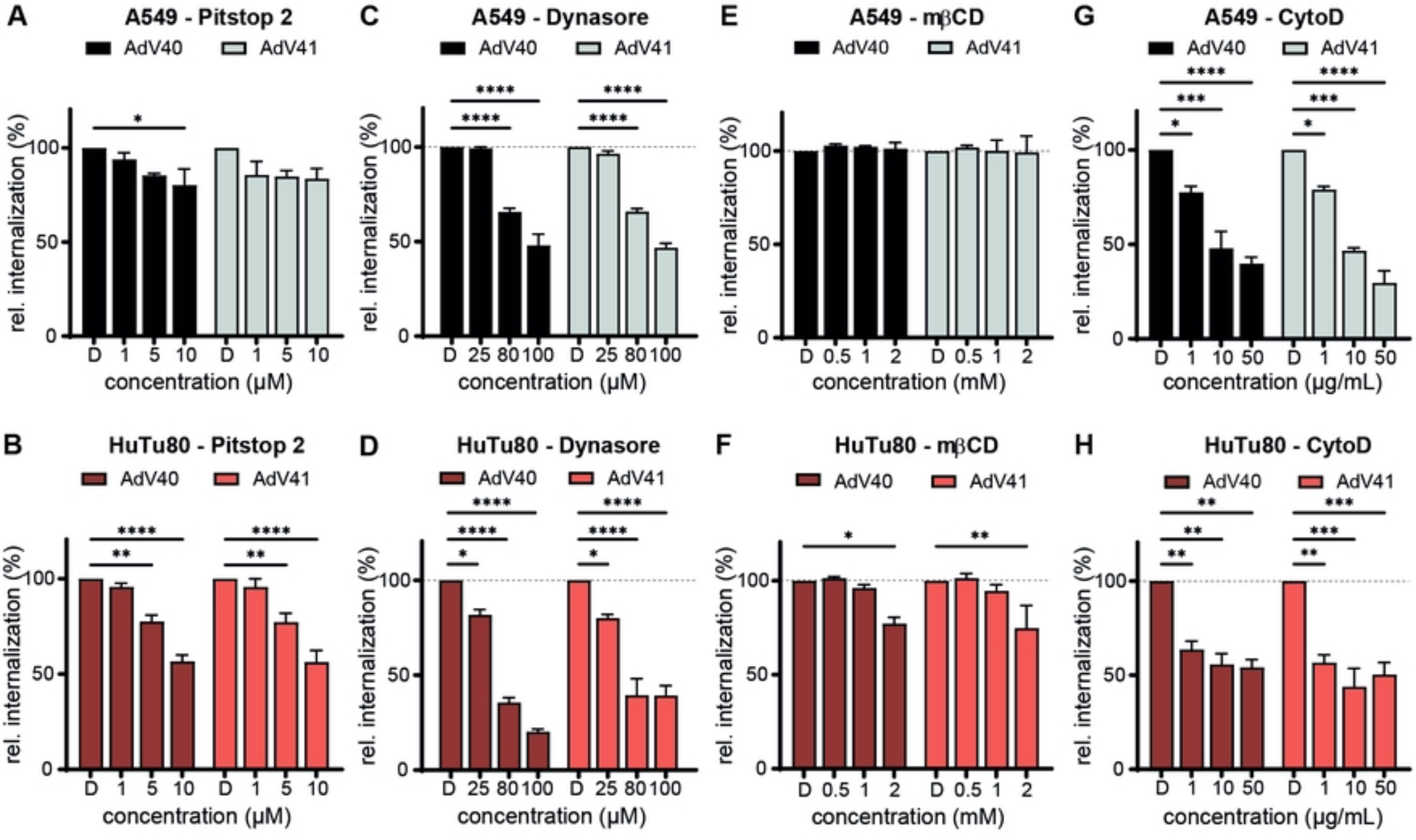
A
A549 - Pitstop 2
AdV40
AdV41
rel. internalization (%)
concentration (µM)
B
HuTu80 - Pitstop 2
C
A549 - Dynasore
D
HuTu80 - Dynasore
E
A549 - mβCD
concentration (mM)
F
HuTu80 - mβCD
G
A549 - CytoD
concentration (µg/mL)
H
HuTu80 - CytoD

Figure 4

bioRxiv preprint doi: https://doi.org/10.1101/2023.03.06.531250; this version posted March 6, 2023. The copyright holder for this preprint (which was not certified by peer review) is the author/funder, who has granted bioRxiv a license to display the preprint in perpetuity. It is made available under aCC-BY 4.0 International license.

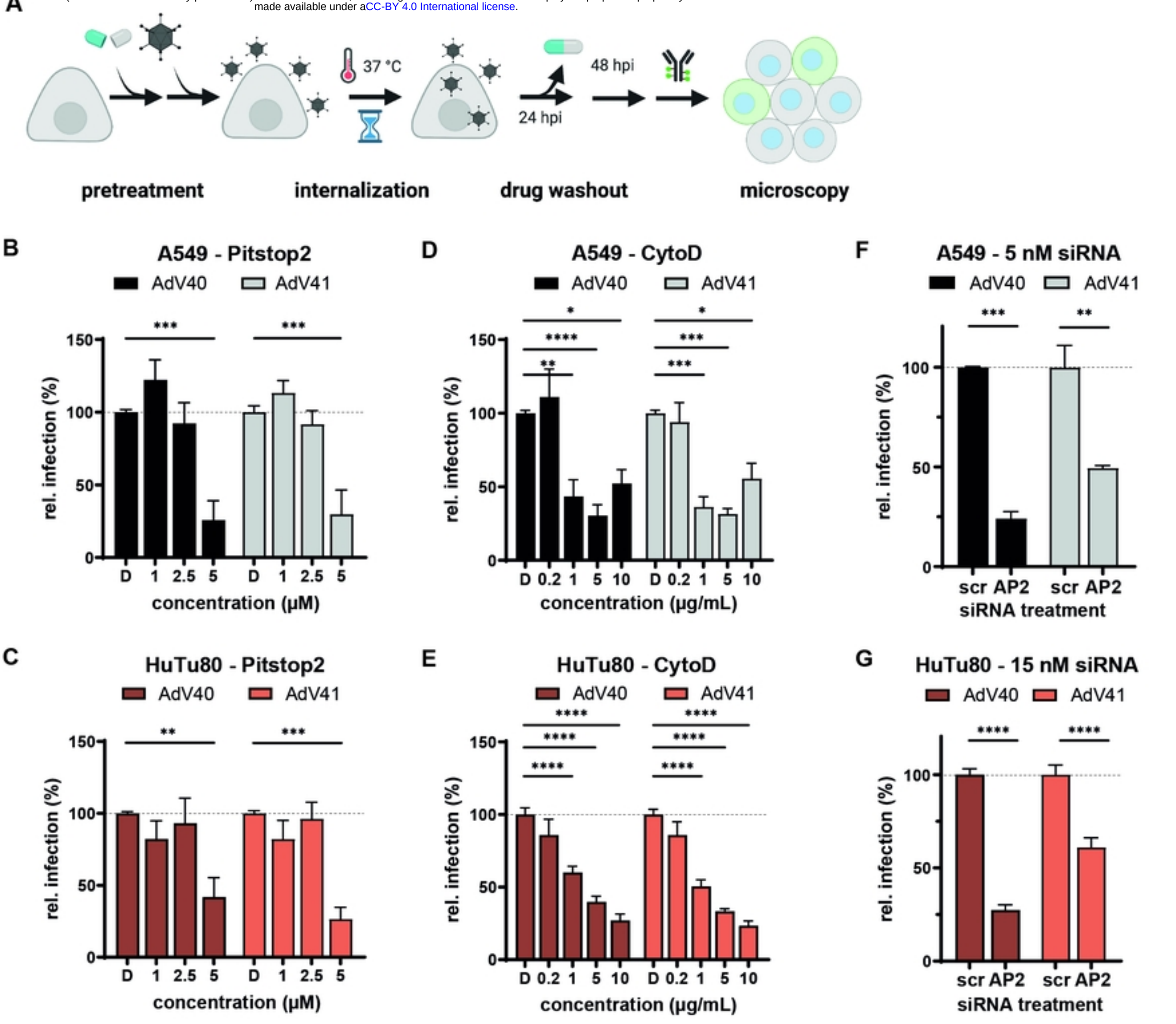

Figure 5